Article

Structural and Mechanical Evolution of Mesoporous Films With Thermal Treatment: The Case of Brij 58 Templated Titania

Diego Fernando Lionello, Paula Y. Steinberg, M. Mercedes Zalduendo,
Galo J. A. A. Soler-Illia, Paula C. Angelomé, and María Cecilia Fuertes

Just Accepted

Structural and Mechanical Evolution of Mesoporous Films With Thermal Treatment: the Case of Brij 58 Templated Titania

Diego F. Lionello[a,b#], Paula Y. Steinberg[a,c#], M. Mercedes Zalduendo[a,c], Galo J. A. A. Soler-Illia[d], Paula C. Angelomé[a*], M. Cecilia Fuertes[a,b*]

[a] Gerencia Química, Centro Atómico Constituyentes, Comisión Nacional de Energía Atómica, CONICET, Av. Gral. Paz 1499, B1650KNA San Martín, Buenos Aires, Argentina.

[b] Instituto Sabato, UNSAM-CNEA, Av. Gral. Paz 1499, B1650KNA San Martín, Buenos Aires, Argentina.

[c] Departamento de Química Inorgánica, Analítica y Química Física, Facultad de Ciencias Exactas y Naturales, Universidad de Buenos Aires, Intendente Güiraldes 2169, Ciudad Universitaria, C1428GA Capital Federal, Argentina

[d] Instituto de Nanosistemas, UNSAM, CONICET, 25 de mayo 1021, 1650 San Martín, Buenos Aires, Argentina.

[#] These authors contributed equally to this work.

* Corresponding authors emails: mfuertes@cnea.gov.ar; angelome@cnea.gov.ar

1
2
3
4
5
6
7
8
9
10
11
12
13
14
15
16
17
18
19
20
21
22
23
24
25
26
27
28
29
30
31
32
33
34
35
36
37
38
39
40
41
42
43
44
45
46
47
48
49
50
51
52
53
54
55
56
57
58
59
60

Abstract

Mesoporous titania thin films (MTTFs) with well ordered cubic array of mesopores were synthesized on glass and silicon substrates using Brij 58 as template. The effect of the thermal treatment and the substrate on the structural parameters (thickness, porosity, pore order, crystallinity) and the mechanical properties of MTTFs were determined by electron microscopy, X-Ray diffraction, Raman spectroscopy, 2D-Small Angle X-Ray Scattering, ellipsometric porosimetry and nanoindentation.

Clear differences in the mesostructural order evolution and crystallization behavior were observed as a function of the substrate and the thermal treatment. In particular, the anatase crystallization process occurs at lower temperatures for samples prepared on silicon when compared with samples prepared on glass, due to the balance between nanocrystals formation, mass diffusion and Na^+ migration from the substrate.

As a consequence of such phenomena, the MTTFs mechanical properties are also dependant on the substrate. For samples prepared on glass the 325 - 350°C range is the optimal annealing temperature to maximize the mechanical properties (E value of 45 GPa), while higher temperatures can be used for the Si supported oxides, to reach E values of 60 GPa.

The obtained anatase crystal dimensions (below 4-5 nm) are restricted by the wall thickness, indicating the chosen thermal treatment prevents mesoporous structure to collapse even when the oxide presents thin walls and small pores, preserving high porosity and high porous ordering. As a consequence, the presented Brij 58 templated MTTFs present smaller crystalline domains than analogous materials with thicker walls. Such properties could be exploited for applications in photocatalysis and titania-based solar cells.

Introduction

Mesoporous TiO_2 thin films (MTTFs) have attracted a great interest during the last years in the materials science community. MTTFs are particularly interesting since they combine the unique properties of TiO_2 with an accessible porosity, controlled thicknesses and have the possibility of the integration in several devices.

In fact, titanium dioxide has many attractive characteristics such as chemical stability, biocompatibility and low-cost processing. As a consequence, it has been used in a wide range of applications from pigments, sunscreens, cosmetics and optical coatings to food additives[1]. Moreover, nanostructured titania has shown many potential applications in photocatalysis[2], photovoltaic devices[3-4], sensors[5], nanoelectrods[6], electronics[7], drug delivery[8] and implants[9]. A few common requirements have to be fulfilled in order to effectively apply nanostructured titania in all the mentioned fields: a well controlled porosity and crystalline structure, high surface area, the possibility to be processed as thin film and high mechanical stability[10-13]. In this sense, MTTFs offer great advantages, since their synthesis is very reproducible and the porosity and pore sizes can be precisely varied by controlling the synthesis and post-synthesis conditions[1].

The combination of sol-gel methods with self-assembly of amphiphilic molecules in the so called Evaporation Induced Self Assembly (EISA)[14] methodology has been the main strategy adopted to build such MTTFs. The first examples of optically uniform mesoporous TiO_2 films, using poly(ethylene oxide)-based on ionic surfactants as structuring agents, were reported in 2001[15-16]. Since those initial reports, a large body of work has been dedicated to study MTTFs, with particular interest in three features: the first stage of the MTTFs formation process, the crystallinity development and the applications in devices[1, 11-12].

Thus, previous papers have been centered in obtaining different pore arrays and sizes and, mainly, highly crystalline frameworks, essential for most of the MTTFs projected applications. In that sense, several characterization techniques have been used to elucidate the role of different synthesis and post synthesis conditions over the final structure of the MTTFs[1], including: Wide Angle X Ray Spectroscopy[17-18], Small Angle X Ray Scattering (SAXS)[17, 19], 2D-SAXS[18, 20-21], interferometry[20], X Ray Diffraction (XRD)[22],X Ray

Absorption (XANES)[23], ellipsometry[24-25] and environmental ellipsometric porosimetry (EEP)[26-27]. By means of such studies it was possible to establish a set of key parameters that determine the final ordering and crystallinity of MTTFs. For example, it was determined that crystallization depends on the thermal treatment[18, 22, 24-25], however, the substrate has also a strong influence on this process. In fact, glass substrate delays the crystallization when compared with silicon substrates[23]; if transparent MTTFs are required, a more complex synthetic path (including a "buffer" non porous TiO_2 layer) is needed to ensure crystallization[26]. Also the thickness seems to have influence on the MTTFs final properties and, in general, thicker films presented higher percentage of porosity, lower density and higher roughness[28]. Furthermore, an increment in the optical band gap for mesoporous titania with respect to dense material was measured and attributed to weak quantum confinement effects derived from the anatase nanoscopic grain size[29].

From the application point of view, the influence of synthesis conditions and post-synthesis processing on the MTTFs properties result crucial. For example, the photocatalytic activity of MTTFs was found to be related to the pore array[30], the morphology of the crystalline porous network and the crystallite size[27, 31]. Interestingly, all these parameters are strongly dependant on the post treatment temperature.

The majority of the published works about MTTFs are dedicated to materials presenting interpore distances of about 10 nm, being the *Im3m* cubic structure produced using Pluronic F127 as template the most commonly reported[4, 17-18, 23-28, 31-35]. This arrangement usually evolves towards the so called "grid-like" structure after thermal treatment; anatase nanocrystals are formed inside the walls with sizes determined by the original interpore distance. Also KLE polymers[1, 36-37] and Pluronic P123[22, 25, 29, 38] have been extensively used as templates for MTTFs, obtaining similar interpore distances as in the F127 case. In contrast, there is scarce information about systems with thinner walls, in which size effects could arise. An extensive work about the first stages of Brij 58 templated films formation and evolution in different environmental conditions was presented by Sanchez's group in 2003[20]. More recently, our group has studied the thermal evolution of Brij 56 templated TiO_2 up to 200°C[21]. However, no insightful studies have been presented in order to elucidate whether pore size or interpore distances could induce significant changes to MTTFs thermal evolution.

Also, there is a lack of information regarding to the mechanical properties of TiO_2 mesoporous systems, which play a major role when applications of MTTFs are envisioned. And, once again, the reported data are limited to systems with ~10 nm interpore distances. Those data, obtained by EEP[4], combining a Love wave platform with EEP[39] or by nanoindentation (NI)[40], demonstrated that Young's modulus changes as a function of porosity, pore dimensions and thermal treatment applied.

In this study, structural changes and mechanical properties of MTTFs templated with Brij 58 copolymer were investigated. The chosen template gives rise to MTTFs with smaller pores and interpore distances than the F127 templated ones, but with the same initial pore array (cubic *Im3m*), allowing a direct comparison between both systems. Glass and silicon were used as substrates for the films, and different calcinations temperatures were applied from 200°C to 450°C. 2D-SAXS and ellipsometric measurements were used to follow the thickness and pore array evolution of the MTTFs as a function of the temperature. Porosity evolution was determined by electron microscopy and EEP, and an extensive study about the system crystallinity was performed by XRD and Raman spectroscopy. All the structural information was related to the MTTFs mechanical properties, determined by nanoindentation.

This knowledge of the relationship between processing and final properties of small pores MTTFs opens the possibility to design and optimize the thermal treatment for the potential application of this controlled porous systems.

Experimental

Synthesis

MTTFs were prepared by a combination of sol-gel and Evaporation Induced Self Assembly (EISA) techniques[20] from a sol containing an inorganic precursor and an organic pore template. The sol was prepared as reported in previous works[20] by mixing $TiCl_4$ (Sigma Aldrich) and absolute ethanol (EtOH, BIOPACK) in a 1:40 molar ratio. The pore template Brij 58® ($[CH_3(CH_2)_{15}(CH_2CH_2O)_{20}OH]$, Merck) and E-pure H_2O (R = 18MΩ.cm^{-1}) were added to the mixture. The final molar composition was 1 $TiCl_4$: 40 EtOH: 10 H_2O: 0.05 Brij 58. The same sol but without the template was prepared to obtain non-mesoporous titania, used as a control.

5

Substrates were cleaned with ethanol before thin film deposition. The as-prepared sol was deposited onto silicon (S) and glass (G) substrates by dip-coating at 2 mm s^{-1} withdrawal speed inside a camera at room temperature and *ca.* 30% relative humidity (RH). These materials were stabilized and calcined in consecutive steps. The stabilization steps consisted of 30 min in a chamber at 50% RH and at room temperature, 30 min at 60°C and 30 min at 130°C. At his point, to obtain thicker films, the materials were subsequently stabilized at 200°C for 30 minutes; thus, a second deposition could be performed avoiding damaging the first layer[41]. Once more, these materials were stabilized up to 200°C before a third layer was deposited and stabilized up to 130°C. All the systems were finally treated at the following calcination temperatures: 200, 250, 300, 325, 350 or 375°C during 2 h (denoted as "2h") with a ramp of 2°C min^{-1} from 130°C. After calcination at 350°C, some of the samples were treated at 375, 400 or 450 °C, during 15 min to induce TiO_2 crystallization[26]. This is a "flash" thermal treatment, denoted as "F". These treatments were designed to produce conditions in which the rate of titania crystallization is greater than the rate of ordered structure deterioration due to extensive mass diffusion[42]. Samples treated at 200 and 250°C were immersed in EtOH for 48 h to extract the surfactant before all measurements.

Characterization

Transmission Electron Microscopy (TEM) images and Selected Area Electron Diffraction (SAED) patterns were obtained with a Philips CM 200 transmission electron microscope. Films were scratched from the substrate and deposited on carbon-coated copper grids.

Field Emission-Scanning Electron Microscopy (FE-SEM) images were obtained with a ZEISS LEO GEMINI field emission electron microscope. Samples were cut into small pieces and mounted on standard aluminum 12.7 mm pin stubs using carbon conductive tape and silver paint, to improve electrical contact. Samples were also characterized using a Philips 515 Electron Microscope equipped with EDS; for the EDS quantification, samples were scratched from the substrate and deposited on carbon conductive tape.

2D-SAXS patterns were acquired at the SAXS2 beamline of Laboratório Nacional de Luz Sincrotrón equipped with a CCD camera as detector, using a 1.55 Å incidence X-ray beam. Sample to detector distance was 73.28 cm and the synchrotron radiation incidence angle

was 3° from the sample surface. Samples were prepared on thin glass slides (ca. 0.15 mm thick) to allow these measurements.

XRD patterns were recorded on a Panalytical Empyrean diffractometer, using Cu Ka_{α} radiation (1.54 Å), a 1° incident beam angle, a 0.38 mm divergence slit and a 15 mm mask. A monochromator was positioned between the sample and the detector. Diffraction patterns were collected from 22.5 to 28° 2θ with a step size of 0.025° and time per step of 5 s. The chosen range corresponds to (101) reflection of anatase, which is the only diffraction peak that is clearly observed in this kind of MTTFs.

Raman scattering measurements were performed at room temperature using a Horiba LabRAMHR Raman system (Horiba Jobin Yvon). An Ar$^+$ laser line at 514.5 nm was used as an excitation source (power output 8 mW). The laser was focused on the sample using a 100× magnification objective which resulted in a laser spot size of 1 μm. Spectra were collected in the wavenumber range from 100 to 800 cm^{-1} on a CCD detector. A monochromator grating of 1800 linesmm^{-1} was selected to obtain a spectral resolution better than 1 cm^{-1}. Acquisition conditions were set to 3 scans and 10 s integration time. Each sample was analyzed by measuring at least 3 different points.

The thickness, porosity and pore size distribution were obtained by EEP. The changes of ellipsometric parameters Ψ and Δ at variable vapor pressure (P/Po) of water at room temperature were measured in a SOPRA GES5A ellipsometer. All the samples were washed with absolute ethanol and dried before measuring. The experimental data was fitted by Winelli software with Forouhi-Bloomer dispersion law[43]. In order to obtain pore size distribution from the adsorption-desorption isotherms using models based on Kelvin equation[44], water contact angle on films were determined by using a Ramé-Hart 190 CA equipment; images were analyzed using Ramé-Hart DROPimage software.

Mechanical properties were measured in thicker samples (300-400 nm thick) by NI using a Nano Indenter Agilent G200 equipped with a XP head and a Berkovich diamond tip with a radius of *ca.* 20 nm. Two sets of experiments were performed for samples on silicon and glass substrates: 1) a batch defined with an array of 5x5 using the ISO method, applying a peak load of 10 mN and a decrement factor of 0.83; 2) the same batch but applying a peak load of 5 mN [45-46]. Measured values at each load were averaged to obtain the final results. Separation between the indents was 25 μm and Poisson's ratio (ν) values of 0.2, 0.22 and

7

0.2 for glass, silicon and mesoporous TiO_2 respectively, were obtained from literature[40]. Strain rate sensitivity (SRS) was also investigated from NI measurements using two methods: constant rate of loading (CRL)[47] and constant strain rate (CSR)[48]. More information is available in the SI.

Results and discussion

In order to study the thermal evolution of macro, meso and microscopic properties of mesoporous TiO_2 thin films, samples were synthesized by dip coating on glass or silicon substrates. Films were stabilized until 130°C and then treated at different temperatures in the 200-450°C range. Two types of thermal treatments were chosen depending on the final desired temperature. For temperatures up to 350°C, a gentle ramp (2 °C min^{-1}) and 2 h of treatment were used; from 400°C, the 350°C samples were used as base and a flash treatment of 15 minutes at the final temperature was applied. Sample calcined at 375°C was treated with the two options, to study the differences between both treatments over the obtained properties.

All studied systems have thicknesses values between 100 and 400 nm, depending on the thermal treatment and the number of layers (3 layers were deposited consecutively to obtained thicker samples for nanoindentation tests).

1) Pore order and thickness evolution

The first step to study the thermal evolution of MTTFs was following the oxide mesoporous structure as a function of temperature. From 2D-SAXS measurements, the type of pore array and its orientation, the interplanar distances and the structure contraction were obtained[1]. Several previous works have dealt with this evolution for MTTFs, but generally only a part of the process was followed: the first minutes after deposition[20] or the crystallization[18, 38].

In **Figure 1 a-e**, 2D-SAXS patterns of MTTFs as-prepared and treated at different temperatures are presented. It can be seen that the porous structure is a body centered cubic *Im3m* phase, oriented with the planes [110] parallel to the substrate, at all studied temperatures. The chosen thermal treatment procedure prevents the thin wall mesoporous

structure to collapse, an improvement over previous results reported in the literature[20].

However, it is important to note that after the treatment at 350ºC the spot corresponding to

the [110] planes is harder to see, indicating that the pore's ordering is partially lost in the

direction parallel to the substrate, a behavior that has been observed previously[18].

As expected, the pore structure contracts in the direction perpendicular to the substrate

when the treatment temperature is increased[1, 20]. In particular, this behavior is similar to the

one reported by Grosso and coworkers[18] for the case of Pluronic F127 templated MTTFs,

that produces pores of around double diameter than the ones studied in this work, which are

around 3-6 nm, depending on the thermal treatment **(see Table S1, SI).** Hence, these results

indicate that the thermal treatment effect over the structure's contraction seems to be
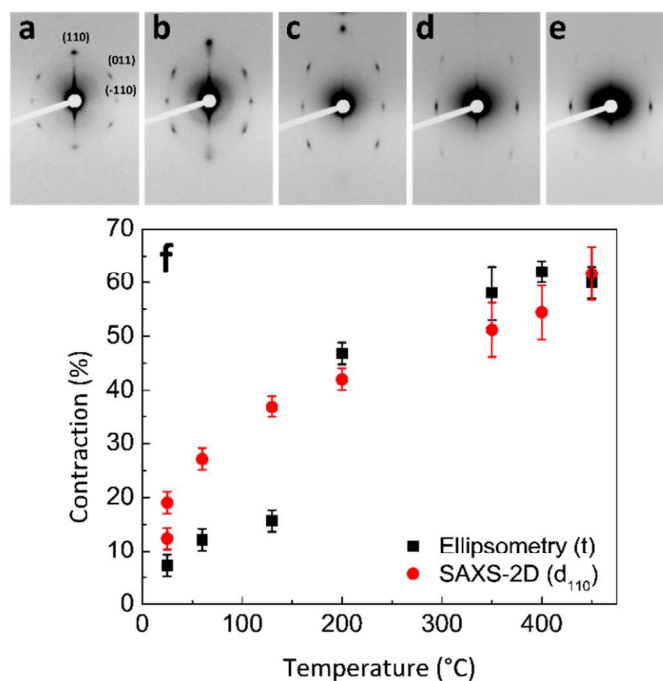
independent from the material's pore size.

Figure 1. 2D-SAXS pattern of samples on glass as a function of processing conditions: (**a**) as prepared, (**b**) 130°C, (**c**) 200°C, (**d**) 350°C and (**e**) 400°C. (**f**) Structural contraction as a function of thermal treatment, obtained by ellipsometry and 2D-SAXS. t=thickness; d_{110}=[110] interplanar distance.

The level of uniaxial contraction of the mesoporous structure can be calculated by

comparing the d_{110} distance (which decreases as a function of temperature) and the d_{-110}

distance, which remains invariable (**Figure S1.a, SI**). Analogously, the percentage of

contraction can be calculated by comparing the film thickness at each temperature, with the

9

one corresponding to the fresh film, determined by ellipsometry (**Figure S1.b, SI**). The

results of these calculations are presented in **Figure 1.f**. It is interesting to note that the film

contracts macroscopically (as determined by ellipsometric measurements) and

microscopically (2D-SAXS results) in the same way. This means all the thickness variation

can be related to the deformation of *Im3m* pore structure in the direction parallel to the

substrate, at mesoscopic scale. Similar results were obtained for the MTTFs deposited on

silicon, indicating that the substrate has not a major effect on such uniaxial contraction.

2) Evolution of porosity and pore sizes

Temperature has influence on the porosity and pore size of mesoporous materials[18, 27]. To

study the effect on the Brij 58 templated samples, EEP measurements were performed. The

obtained water adsorption-desorption isotherms are presented in **Figure 2** for samples
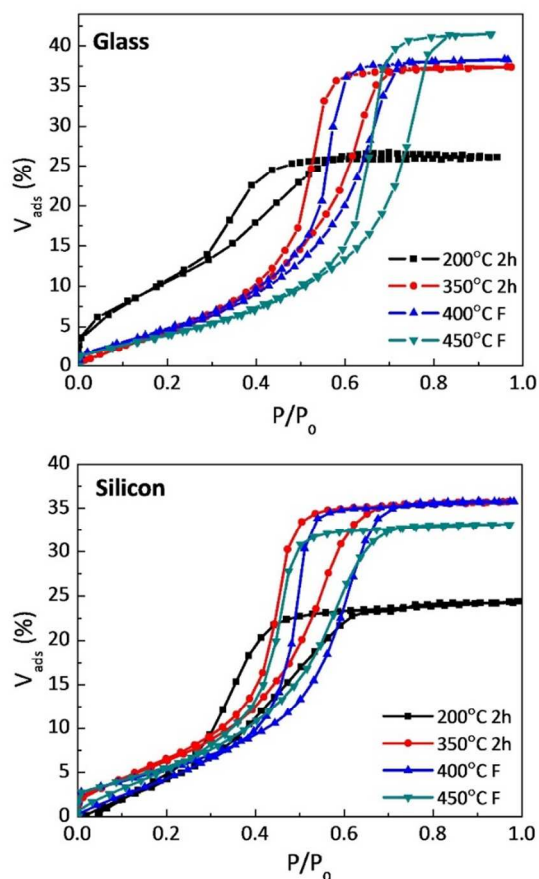
prepared on silicon and glass.

Figure 2. Water adsorption-desorption isotherms obtained by EEP for selected TiO$_2$-Brij58 films deposited on
silicon and glass, as a function of treatment temperature.

The porous volume (see **Table S1, SI**) is similar for almost all samples thermally treated at temperatures higher than 250°C: (38 ± 3) % for samples deposited on glass, and (33 ± 3) % for samples prepared on silicon. Samples treated at 200°C and then immersed in EtOH to extract the template are less porous (around 25 %); this behavior is attributed to the lower degree of contraction of the structure (observed by 2D-SAXS, **Figure 1.c**) that give rise to less accessible oxides.

A hysteresis loop (type IV isotherm), which is related to the capillary condensation taking place in the mesopores[49-50], is observed for all the studied films (**Figure 2**). For samples prepared on glass, the isotherms changes gradually from H2 (which indicates the presence of pores connected by smaller openings, or *ink-bottle* pore structure) to H1 (cylindrical pore geometry) type[50]; this variation of the isotherm shape was previously associated with the generation of a more contracted structure usually called *grid-like* in the literature[18, 27]. Similar trends have been previously observed for mesoporous TiO_2 films with larger pores and thicker walls, templated with F127[4, 24, 27]. This structural change is very marked between 400 and 450°C for samples deposited on glass, and is not observed for samples prepared on Si substrates.

From the isotherms analysis based on the Kelvin equation[44], an increment of pore and neck sizes with the temperature can be observed. On Si substrates, the pore diameter changes from (2.0 ± 0.1) to (4.0 ± 0.1) nm and the neck diameter changes from (1.7 ± 0.1) to (3.1 ± 0.1) nm. For films deposited on glass, a more pronounced displacement of adsorption and desorption branches can be seen, indicating a more significant variation in pore and neck sizes with the temperature and the change to a more contracted pore array. On this substrate, pore diameter changes from (2.6 ± 0.1) to (8.2 ± 0.1) nm and neck diameter changes from (1.7 ± 0.1) to (5.6 ± 0.1) nm. Nevertheless, it is important to note that the obtained values for samples that present H1 type isotherms (the ones treated at higher temperatures) are not a good indication of the real pore size since these pores present a more cylindrical shape, which is not taken into account by Kelvin's equation. The complete set of data is presented in **Table S1, SI.**

The dissimilar effect of the thermal treatment over the meso-order structure observed for the two substrates can be attributed to a competition between two processes: the atomic-

scale crystallization and the nanometer-scale structural change due to mass diffusion[42]. It was previously reported that these two mechanisms have activation energies with the same order of magnitude for P123 templated titania [42]. The crystallization process in the Brij 58 templated MTTFs will be discussed in the next sections.

2) TiO₂ walls thermal evolution

2.1) TEM-SAED studies

Electronic microscopy characterization was performed in order to follow the local changes in the porosity and the oxide wall structure as a function of temperature. TEM and SAED results are presented in **Figure 3**, and additional SEM surface images can be seen in **Figure S2 (SI).**
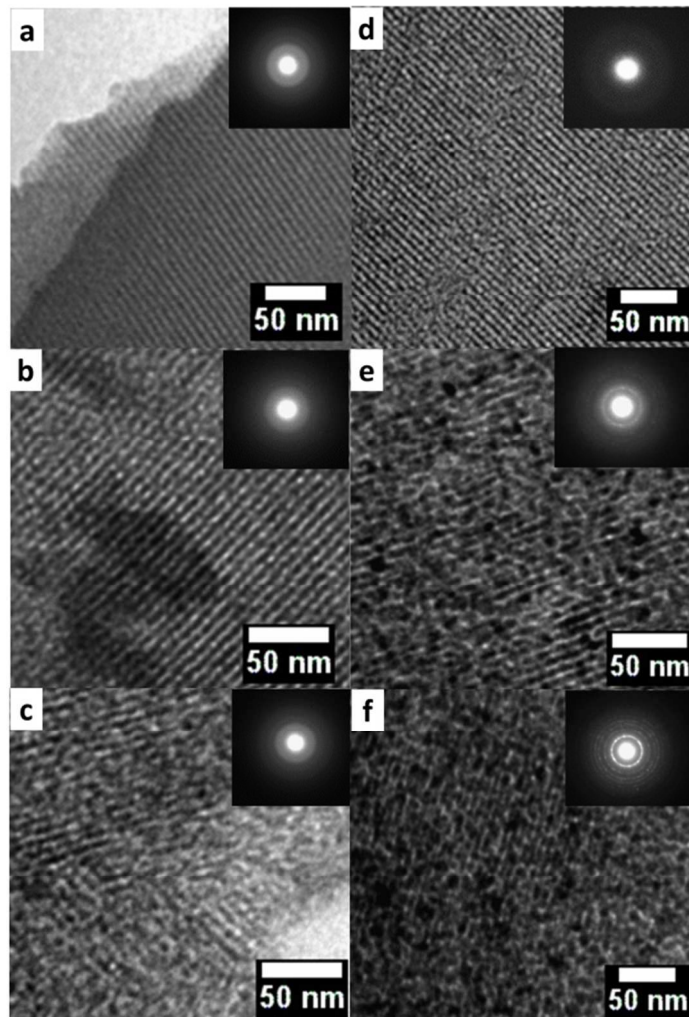
Figure 3. TEM images and SAED diagrams (insets) of Brij 58 templated TiO₂ thin films: (a) 200°C G, (b) 350°C G, (c) 400°C G, (d) 200°C S, (e) 350°C S, (f) 400°C S.

12

From the presented images, it is clear that either samples deposited on glass or silicon present well-ordered *Im3m* mesopores arrays for all essayed temperatures, in concordance with 2D-SAXS results. In the case of silicon substrate, very small anatase crystals show up as dark spots in TiO_2 walls zones for samples treated at $T \geq 350^oC$, coincidently with the appearance of anatase diffraction spots in the SAED diagrams (**Figure 3.e and f**). For films deposited on glass, anatase crystals could not be detected by SAED at any of the studied temperatures.

2.2) XRD studies

Figure 4 exhibits XRD results; the presence of crystalline anatase phase is evidenced by the appearance of the (101) diffraction peak at 25.4°2θ. The crystalline phase is observed from 350°C for samples prepared on silicon, in agreement with the SAED results. For samples deposited on glass, the anatase peak is observed from 375°C (2 h). This apparent contradiction with SAED results can be attributed to the difference in the sample amount studied by each technique: SAED collects information from $\sim 1\ \mu m^2$ of sample while the data obtained by XRD comes from much bigger areas ($\sim 1\ cm^2$).

The difference in the TiO_2 crystallization temperature as a function of the substrate has been previously shown for F127 templated titania, and it was attributed to the Na^+ diffusion from the glass substrate that delays the crystallization process[23].
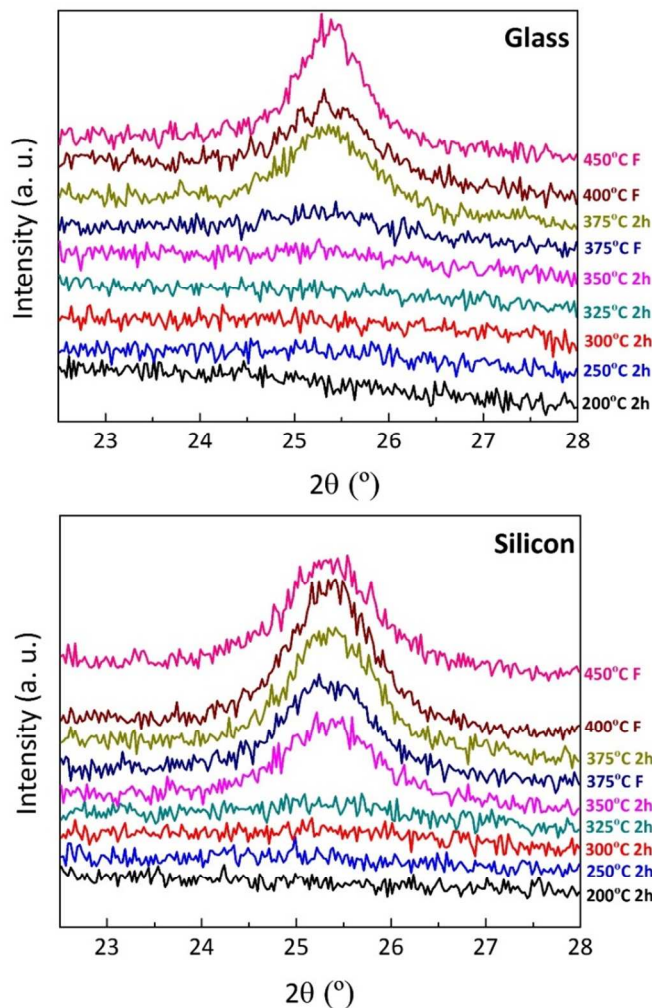
Figure 4. XRD of mesoporous titania samples prepared on glass and silicon treated from 200°C to 450°C (as indicated in the labels), showing the angular region for (101) anatase diffraction peak.

Figure 5 shows the crystallite sizes calculated from the (101) peak using the Scherrer equation. Anastase nanocrystals grow after the transition temperature for each substrate is reached, and remain at almost the same size for higher temperatures. The largest crystalline domain size obtained for both substrates is in the 4 - 5 nm range, very similar to the wall thickness[20] and clearly smaller than the values obtained for Pluronic F127 templated TiO_2 (crystallite sizes from 7 to 8.5 nm)[23] and P123 templated TiO_2 (values between 8.5 and 10 nm)[42] treated at similar temperatures on Si substrates.

These results indicate that anatase crystal dimensions are restricted by wall thickness and that Brij 58 templated mesoporous thin films present smaller crystalline domains than the analogous materials with thicker walls.
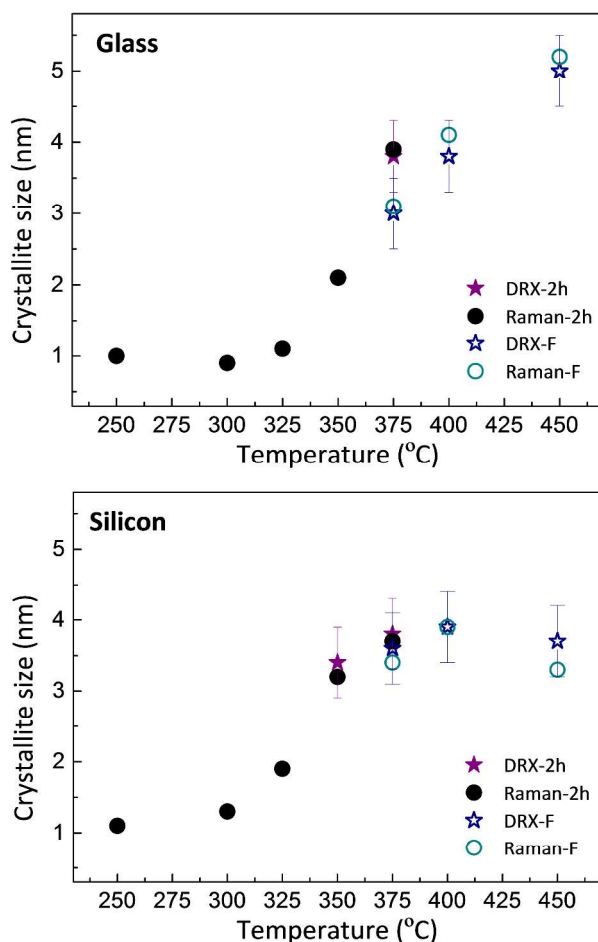
14

Figure 5. Crystallite sizes calculated from the XRD data and the Raman signals for samples prepared on glass and silicon treated at different temperatures.

2.3) Raman studies

In order to better understand the crystallization behavior, Raman spectroscopy studies were performed on the same systems. In a previous work, it was possible to study the Ti (IV) local symmetry and accurately quantify the crystalline fraction of the inorganic walls by analyzing the pre-edge zone in Ti XANES spectra. This technique demonstrated that a small fraction of anatase-like domains is present from temperatures as low as 200°C, for F127 templated TiO_2, even when no anatase peaks are present in XRD patterns[23]. In this work, Raman spectroscopy was used with the same purpose: to get information about the local environment of Ti(V) centers, which is intimately related to the degree of crystallization of MTTFs, by studying the Ti-O vibrations and thus, obtain information

15

about the degree of crystallization of MTTFs.[51] In fact, Raman spectra provide a much better insight into the structure with respect to diffraction techniques and are used as a benchmark for detecting the presence of crystalline titania phases.[51]

The obtained Raman spectra are presented in **Figure 6.** In all samples, the most intense anatase signal corresponding to Eg (υ6) active Raman mode can be identified. However, for higher temperatures, the Eg signal is more intense and more signals are visible in the spectra, indicating a higher degree of crystallinity. Importantly, no signs of the rutile phase are detected, as expected.[52-53]
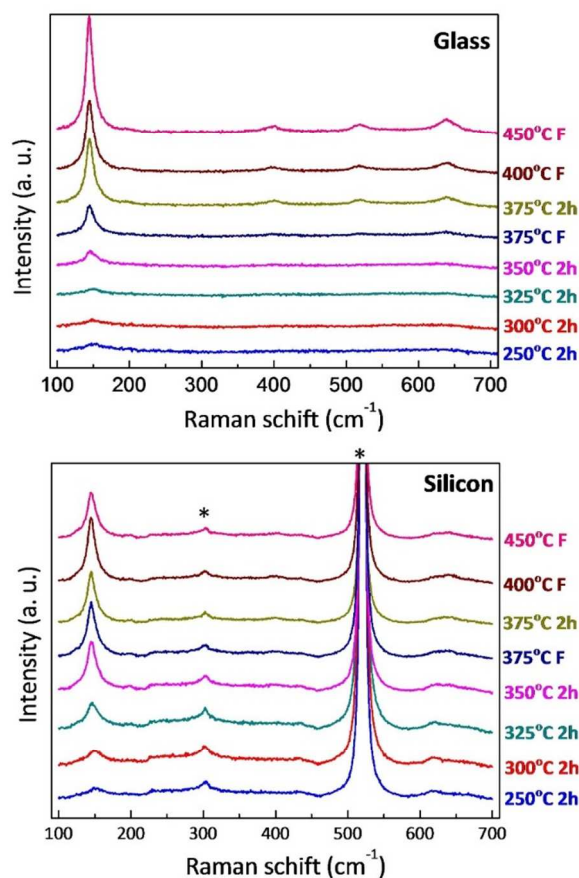

Figure 6. Raman spectra of Brij 58-templated mesoporous titania films on glass and silicon substrates as a function of thermal treatment. The bands marked with * correspond to the Si substrate.

The Eg (υ6) band is located at 144 cm^{-1} for pure bulk TiO_2 anatase crystal[54], and it has been demonstrated that when the crystal size is diminished, its full width at half maximum

(FWHM) increases, its position is displaced towards higher wavenumbers and its intensity decreases.[52, 55]

The evolution of Eg peak position and FWHM for samples treated from 250 to 450°C and deposited on both substrates is shown in **Figure S3 (SI)**. The Raman data can be combined with DRX data to predict the crystal size of small anatase crystals (in this case < 3 nm) that cannot be detected by XRD (see more of such calculations details in the SI).[56] The calculated crystalline domain sizes obtained from these measurements are shown with those obtained using XRD in **Figure 5.**

The most remarkable change in crystallite sizes detected by Raman starts at 300°C or 325°C when using silicon or glass substrates, respectively. Those transition temperatures are lower than the ones determined by XRD (350ºC for Si and 375ºC for glass). The difference between Raman and XRD techniques consists in the minimal crystal-like order extension that may generate a detectable signal. In particular, Raman spectroscopy is able to detect short range order, which means that the presence of anatase-like domains is identified at a lower temperature than by XRD.

It is also significant to note that for samples prepared on glass the crystalline domain size measured using both techniques increases from around 4 nm at 400°C to more than 5 nm at 450°C (see **Figure 5**). This behavior could be related with the previously observed evolution of the mesoporous order (**Figure 2**). In fact, *Im3m* structure presents a highly restrictive geometry for crystal growth. A structure with cylindrical pores, on the contrary, allows crystal growth by diffusive sintering in the direction parallel to the channels, formed by the rearrangement of cubically ordered pores. A similar phenomenon was previously observed for mesostructured titania with larger pores[22].

For samples prepared on Si, the crystalline domain size remains almost constant from 375°C and beyond, indicating that the *Im3m* pores structure is preserved even at the highest explored temperatures, and possibly constrains the anatase crystal growth. The preservation of the cubic mesopore structure with the flash thermal treatment previously shown by EEP could be related to the fact that anatase nanocrystals appear at lower temperatures. These nanocrystals generate stiffer walls than those obtained for MTTFs on glass, whose walls have a more amorphous character at the same temperatures. This amorphous character is

17

possibly associated with the Na^+ diffusion from the substrate[23, 57]. This delay in the crystallization process allows the nanometer-scale structural changes due to mass diffusion. Another interesting observation is related to the difference, for both substrates, in the crystallization behavior for samples prepared by flash thermal treatments. For samples prepared on Si, the final crystalline domain size is reached after 2 h at 350°C, so additional flash thermal treatment at higher temperatures or the 2h treatment at 375°C do not significantly change the crystallite size, even though the total crystalline fraction rises[23]. In fact, both treatments at 375°C (F and 2h) generate approximately the same crystallite size (near 4 nm). For samples prepared on glass substrates, the 375°C 2 h treatment seems to be enough to obtain the maximum crystallite size for the samples with *Im3m* mesopore order (around 4 nm). On the other hand, when the mesoporous order transforms to a more contracted structure (at T > 400°C), the anatase crystals can grow during flash treatment up to 5 nm, and the crystallite size limit imposed by the wall thickness of the *Im3m* pore structure is no longer observed.

4) Mechanical properties

It is well known that nanosized crystallites could affect the mechanical behavior, generating plastic ceramics even at room temperature[58-59]. In addition, for mesoporous materials, it was reported a slight variations in the Young´s modulus as a function of the mesopore order[60] and the pore sizes[40].

The global effect of the thermal treatment in the mechanical properties of Brij 58 templated MTTFs on both substrates was determined by nanoindentation. Load-displacement data were analyzed to obtain indentation modulus (E) of MTTFs. As an example, the measured curves for MTTFs on Si treated at 350°C are presented in **Figure 7.a**, together with a SEM image of the tip mark after the indentation test. The very low surface rugosity for these samples (less than 5 nm) makes it possible to obtain reproducible E values in all tested area, of around 4 cm^2. Interestingly, cracking never occurs during the nanoindentation testing of these samples. This fact could be connected to the relaxation of the applied tension at the vertices of the tip marks due to the presence of pores, improving the fracture toughness of these materials[61].
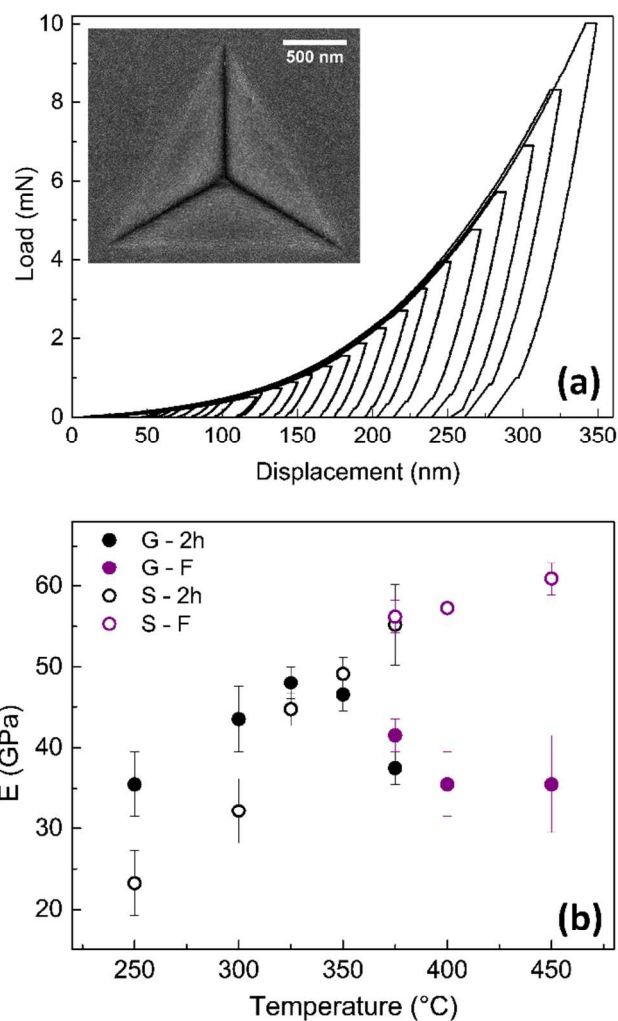
Figure 7. (a) Nanoindentation curves obtained for samples prepared on Si and treated at 350°C. Inset: SEM micrograph of a tip mark on the same sample. (b) Indentation moduli as a function of temperature for films deposited on glass (G) and silicon (S).

The obtained moduli as a function of temperature for both substrates are presented in **Figure 7.b**.In all cases, E values are lower than the ones measured for dense titania (around 130-150 GPa for amorphous TiO_2 and 160-180 GPa for the anatase phase)[46] due to the sample porosity[61].

For samples prepared on Si, the measured E values increase monotonously from 20 to 60 GPa. As has been shown in the previous sections, for these samples there are not significant changes in the porosity or the mesopore structure as a function of temperature. As a consequence, the observed E variation can be associated with an increment in the TiO_2walls

19

condensation and in the anatase phase concentration, even though no variation of the crystallite sizes for temperatures higher than 375°C are observed.

For MTTFs prepared on glass, E values increase as a function of temperature in the 250°C - 325°C range, as the TiO_2 walls condensate and the microporosity inside these walls diminishes. But remarkably, E values starts to go down from this temperature until a plateau is reached at 400°C. For the highest temperatures explored, the measured E values are around 35 GPa, almost a half of the values obtained for samples prepared on Si and treated at the same temperature. Curiously, the porosity and the crystalline domain size of glass supported samples are pretty similar to those obtained for Si supported samples.

In the late 80´s, it was discovered that nanocrystalline oxides may presented extensive ductility or even superplasticity effects when the size of the nanocrystals is reduced[62-64]. More recently, for mesoporous films, Lancelle-Beltran *et al.* report a reduction in E values at high temperatures of thermal treatment for F127 templated TiO_2[4], determined from ellipsometric porosimetry measurements[44]. These authors attributed the E values behavior at high temperatures to the full crystallization of the inorganic network which transforms the bulk amorphous TiO_2 into a polydomain nanocrystalline suprastructure that exhibits less rigidity due to superplasticity appearance. This phenomenon is not observed in **Figure 7** for Si supported samples that have similar crystalline domain sizes than samples on glass, so this is a strong indicator that this enhanced plasticity on glass is not a consequence of the small domain sizes.

Even though, to confirm this hypothesis, several indentations were performed and different models were used [47-48, 65-66] to obtain the strain rate sensibility (SRS) for the synthesized films. The exponent *m* of the SRS is an indicator of the materials plasticity degree (more information in the SI). The exponent *m* can vary between 0 and 1, the limits for perfectly brittle and perfectly ductile behaviour, respectively.[65] Although room temperature *m* values of ceramics are rarely measured, as it is assumed that $m \approx 0$, conventional ceramics and directionally bonded materials are considered superplastic if they achieve *m* values around 0.3[59]. In the particular case of nanostructured titania, NI measurements were published by Mayo *et al.*, who found that *m* increases for grain sizes below 30 nm.[64] However, the highest *m* value they have found is 0.04, far from the superplasticity region. In the case of the films synthetized in this work, the highest *m* value measured is 0.06, for Si supported

20

films treated at 400°C (see more details in the SI). In conclusion, the enhanced plasticity measured for Brij 58 templated MTTFs prepared on glass cannot be attributed to the presence of anatase nanocrystals.

A different approach was proposed by Yaghoubi *et al*, who studied the mechanical behavior as a function of thermal treatment of TiO_2 granular thin films prepared on glass and quartz.[57] They observed a decrease in hardness and E (measured using NI) for thermally treated samples at temperatures higher than 300°C; they attributed this phenomenon to the thermal diffusion of Na^+ from the glass substrate. The authors detected increasing amount of Na^+ in the titania film surface with the temperature treatment using XPS, similar results were obtained later by another group.[53] The Na^+ ions diffuse inside the oxide and replace some of the high strength Ti-O-Ti bonds with weaker Ti-O-Na bonds. The Na^+ diffusion inside the titania films is a very plausible explanation of the decrease in E values observed for glass supported films. This ionic diffusion also explains the delay in the crystallization process observed by Raman spectroscopy. The hypothesis of Na^+ diffusion was checked by performing NI tests on titania films deposited on fused quartz (substrate without Na^+); in this case, the authors found that samples did not exhibit that hardness and modulus decrease.

To confirm the hypothesis of sodium migration from the substrate in Brij 58 templated MTTFs, EDS measurements were performed on scratched films supported on carbon conductive tape. For Si supported samples, no Na signals are observed, as expected. Notwithstanding, Na signals are present for samples deposited on glass, for all studied temperatures **(Figure S5, SI).** Since the Si signal from the scratched glass substrate is also observed and glass also contains Na, these measurements are not conclusive. However, the Na/Si ratio is much higher in the scratched films than in the glass substrate, indicating a high concentration of Na^+ inside the titania film (see the results of the Na, Si and Ti quantification in **Table S3, SI**). Consequently, the most feasible explanation of the E decrease at temperatures beyond 325°C is the presence of Na^+ in the TiO_2 structure.

In this direction, it is interesting to note that samples on glass thermally treated at 375°C for 2 h have a lower E value that samples with a flash treatment at the same temperature; the larger time at high temperature could possible generate the diffusion of a higher amount of Na inside de TiO_2 structure, with the consequence of the reduction of the E value.

In short, 325 - 350°C range is the optimal annealing temperature to maximize the mechanical properties of Brij 58 templated TiO_2 films prepared on glass. For the same material prepared on Si, the best mechanical properties are obtained after thermal treatment at higher temperatures. Moreover, for MTTFs deposited on Si, higher E values can be obtained, reaching up to 60 GPa, while a maximum value of around 45 GPa can be obtained for samples prepared on glass.

Conclusions

In this work, the structural parameters and mechanical properties evolution of Brij 58 templated MTTFs with the thermal treatment was presented. This evolution was measured for films prepared on glass and silicon substrates, and clear differences in the crystallization and mechanical behavior as a function of the substrate were observed.

By means of 2D-SAXS and ellipsometry measurements, it was demonstrated that thermally treated films contract macroscopically and microscopically in the same way: all the thickness variation can be related to the deformation of *Im3m* pore structure in the direction parallel to the substrate. This behaviour was previously found for samples with pores of around double diameter than the ones studied in this work and thus, these results indicate that the contraction behavior is independent on the pore size[18].

Type IV isotherms, typical of mesoporous materials, was measured for all studied systems, with porosities in the range 25-35%, depending on the thermal treatment. For samples prepared on glass, the isotherms changes gradually from H2 to H1 type as a consequence of the contraction of the mesostructure; this structural change is very marked between 400 and 450°C. Remarkably, this phenomenon is not observed for samples prepared on Si substrates. These differences in the mesostructural order evolution are attributed to the atomic-scale crystallization: this process occurs at lower temperatures for samples prepared on Si than in samples prepared on glass. In the case of samples prepared on Si, the early stiffening of the titania walls minimize the structural changes due to mass diffusion. For samples prepared on glass, on the other hand, crystallization is not favored at lower temperatures and thus, mass diffusion can occur, giving rise to the more contracted structures.

Interestingly, the obtained anatase crystal dimensions (4-5 nm, at higher temperatures) are restricted by the wall thickness. This means that the chosen thermal treatment procedure prevents mesoporous structure to collapse even when containing thin walls and small pores, preserving high porosity and nanocrystalline walls. As a consequence, the presented Brij 58 templated MTTFs present smaller crystalline domains than the analogous materials with thicker walls.

Moreover, the effect of the thermal treatment in the mechanical properties of samples prepared on both substrates was investigated. For samples prepared on Si, the obtained E values increased from 20 to 60 GPa; this variation is associated with an increment in the TiO_2 walls condensation and in the anatase phase concentration as a function of temperature. For MTTFs prepared on glass, E values increase in the 250 - 325°C range, as the TiO_2 walls condensate and the microporosity inside these walls diminishes, but E values starts to reduce from this temperature until a plateau is reached at 400°C. As the porosity and the crystalline domain size of glass supported samples are similar to those obtained for Si supported samples, the most feasible explanation for such E decrease is the presence of Na^+ (that diffuses from the substrate) in the TiO_2 structure. As a consequence, for samples prepared on glass the 325 - 350°C range is the optimal annealing temperature to maximize the mechanical properties, while higher temperatures can be used for the Si supported oxides, demonstrating the importance of the substrate on the MTTFs mechanical properties behavior.

Finally, it is important to note that the obtained MTTFs are nanocrystalline, with very small crystal domains included within a highly porous array of well-ordered small pores. Such interesting and differential properties could be exploited for applications in photocatalysis and titania-based solar cells[1, 26].

Supporting Information

Porosity, pore diameter, interplanar pore distances and film thickness as a function of substrate and temperature. SEM images. Theory and experimental details related to Raman spectroscopy for size determination of anatase nanocrystals. EDS spectra. Theory, experimental details and measurements related to strain rate sensibility.

References

1.   Soler-Illia, G. J. A. A.; Angelomé, P. C.; Fuertes, M. C.; Grosso, D.; Boissiere, C., Critical Aspects in the Production of Periodically Ordered Mesoporous Titania Thin Films. *Nanoscale* **2012**, *4*, 2549-66.

2.   Choi, H.; Sofranko, A. C.; Dionysiou, D. D., Nanocrystalline TiO2 Photocatalytic Membranes with a Hierarchical Mesoporous Multilayer Structure: Synthesis, Characterization, and Multifunction. *Adv. Funct. Mater.* **2006**, *16*, 1067-1074.

3.   Grätzel, M., Conversion of Sunlight to Electric Power by Nanocrystalline Dye-Sensitized Solar Cells. *J. Photochem. Photobiol., A* **2004**, *164*, 3-14.

4.   Lancelle-Beltran, E.; Prené, P.; Boscher, C.; Belleville, P.; Buvat, P.; Lambert, S.; Guillet, F.; Boissière, C.; Grosso, D.; Sanchez, C., Nanostructured Hybrid Solar Cells Based on Self-Assembled Mesoporous Titania Thin Films. *Chem. Mater.* **2006**, *18*, 6152-6156.

5.   Panjawi, N.; Naik, A.; Warwick, M. E. A.; Hyett, G.; Binions, R., The Preparation of Titanium Dioxide Gas Sensors by the Electric Field Assisted Aerosol Cvd Reaction of Titanium Isopropoxide in Toluene. *Chem. Vap. Deposition* **2012**, *18*, 102-106.

6.   Faustini, M.; Marmiroli, B.; Malfatti, L.; Louis, B.; Krins, N.; Falcaro, P.; Grenci, G.; Laberty-Robert, C.; Amenitsch, H.; Innocenzi, P.; Grosso, D., Direct Nano-in-Micropatterning of TiO2 Thin Layers and Tio2/Pt Nanoelectrode Arrays by Deep X-Ray Lithography. *J. Mater. Chem.* **2011**, *21*, 3597-3603.

7.   Martinez, E. D.; Granja, L.; Bellino, M. G.; Soler-Illia, G. J. A. A., Electrical Conductivity in Patterned Silver-Mesoporous Titania Nanocomposite Thin Films: Towards Robust 3D Nano-Electrodes. *Phys. Chem. Chem. Phys.* **2010**, *12*, 14445-14448.

8.   Bass, J. D.; Grosso, D.; Boissiere, C.; Belamie, E.; Coradin, T.; Sanchez, C., Stability of Mesoporous Oxide and Mixed Metal Oxide Materials under Biologically Relevant Conditions. *Chem. Mater.* **2007**, *19*, 4349-4356.

9.   Lilja, M.; Forsgren, J.; Welch, K.; Åstrand, M.; Engqvist, H.; Strømme, M., Photocatalytic and Antimicrobial Properties of Surgical Implant Coatings of Titanium Dioxide Deposited Though Cathodic Arc Evaporation. *Biotechnol. Lett* **2012**, *34*, 2299-2305.

10.   Zhang, R.; Elzatahry, A. A.; Al-Deyab, S. S.; Zhao, D., Mesoporous Titania: From Synthesis to Application. *Nano Today* **2012**, *7*, 344-366.

11.   Gu, D.; Schuth, F., Synthesis of Non-Siliceous Mesoporous Oxides. *Chem. Soc. Rev.* **2014**, *43*, 313-344.

12.   Li, W.; Wu, Z.; Wang, J.; Elzatahry, A. A.; Zhao, D., A Perspective on Mesoporous TiO2 Materials. *Chem. Mater.* **2014**, *26*, 287-298.

13.   Bagheri, S.; Mohd Hir, Z. A.; Yousefi, A. T.; Abdul Hamid, S. B., Progress on Mesoporous Titanium Dioxide: Synthesis, Modification and Applications. *Microporous Mesoporous Mater.* **2015**, *218*, 206-222.

14.   Brinker, C. J.; Lu, Y.; Sellinger, A.; Fan, H., Evaporation-Induced Self-Assembly: Nanostructures Made Easy. *Adv. Mater.* **1999**, *11*, 579-585.

15.   Yun, H. S.; Miyazawa, K.; Zhou, H. S.; Honma, I.; Kuwabara, M., Synthesis of Mesoporous Thin TiO2 Films with Hexagonal Pore Structures Using Triblock Copolymer Templates. *Adv. Mater.* **2001**, *13*, 1377-1380.

16.   Grosso, D.; Soler-Illia, G. J. A. A.; Babonneau, F.; Sanchez, C.; Albouy, P. A.; Brunet-Bruneau, A.; Balkenende, A. R., Highly Organized Mesoporous Titania Thin Films Showing Mono-Oriented 2D Hexagonal Channels. *Adv. Mater.* **2001**, *13*, 1085-1090.

17.   Wang, J.; Li, H.; Li, H.; Zuo, C.; Wang, H., Thermal Stability and Optimal Photoinduced Hydrophilicity of Mesoporous TiO2 Thin Films. *J. Phys. Chem. C* **2012**, *116*, 9517-9525.

18.   Grosso, D.; Soler-Illia, G. J. A. A.; Crepaldi, E. L.; Cagnol, F.; Sinturel, C.; Bourgeois, A.; Brunet-Bruneau, A.; Amenitsch, H.; Albouy, P. A.; Sanchez, C., Highly Porous TiO2 Anatase Optical Thin Films with Cubic Mesostructure Stabilized at 700 °C. *Chem. Mater.* **2003**, *15*, 4562-4570.

19.   Luca, V.; Bertram, W. K.; Sizgek, G. D.; Yang, B.; Cookson, D., Delineating the First Few Seconds of Supramolecular Self-Assembly of Mesostructured Titanium Oxide Thin Films through Time-Resolved Small Angle X-Ray Scattering. *Langmuir* **2008**, *24*, 10737-10745.

20.   Crepaldi, E. L.; Soler-Illia, G. J. A. A.; Grosso, D.; Cagnol, F.; Ribot, F.; Sanchez, C., Controlled Formation of Highly Organized Mesoporous Titania Thin Films: From Mesostructured Hybrids to Mesoporous Nanoanatase Tio2. *J. Am. Chem. Soc.* **2003**, *125*, 9770-9786.

21.   Gonzalez Solveyra, E.; Fuertes, M. C.; Soler-Illia, G. J. A. A.; Angelomé, P. C., 2D-SAXS in Situ Measurements as a Tool to Study Elusive Mesoporous Phases: The Case of p6mm TiO2. *J. Phys. Chem. C* **2017**, *121*, 3623-3631.

22.   Choi, S. Y.; Mamak, M.; Speakman, S.; Chopra, N.; Ozin, G. A., Evolution of Nanocrystallinity in Periodic Mesoporous Anatase Thin Films. *Small* **2005**, *1*, 226-232.

23.   Angelomé, P. C.; Andrini, L.; Calvo, M. E.; Requejo, F. G.; Bilmes, S. A.; Soler-Illia, G. J. A. A., Mesoporous Anatase Tio2 Films: Use of Ti K XANES for the Quantification of the Nanocrystalline Character and Substrate Effects in the Photocatalysis Behavior. *J. Phys. Chem. C* **2007**, *111*, 10886-10893.

24.   Bass, J. D.; Grosso, D.; Boissiere, C.; Sanchez, C., Pyrolysis, Crystallization, and Sintering of Mesostructured Titania Thin Films Assessed by in Situ Thermal Ellipsometry. *J. Am. Chem. Soc.* **2008**, *130*, 7882-7897.

25.   Choi, S. Y.; Mamak, M.; Ozin, G. A.; Peiris, F. C., Exploring the Thermal Transformation of Mesoporous Titania Using Spectroscopic Ellipsometry. *Phys. Status Solidi A* **2008**, *205*, 825-828.

26.   Violi, I. L.; Perez, M. D.; Fuertes, M. C.; Soler-Illia, G. J. A. A., Highly Ordered, Accessible and Nanocrystalline Mesoporous TiO2 Thin Films on Transparent Conductive Substrates. *ACS Appl. Mater. Interfaces* **2012**, *4*, 4320-4330.

27.   Sakatani, Y.; Grosso, D.; Nicole, L.; Boissiere, C.; de A. A. Soler-Illia, G. J.; Sanchez, C., Optimised Photocatalytic Activity of Grid-Like Mesoporous TiO2 Films: Effect of Crystallinity, Pore Size Distribution, and Pore Accessibility. *J. Mater. Chem.* **2006**, *16*, 77-82.

28.   Henrist, C.; Dewalque, J.; Mathis, F.; Cloots, R., Control of the Porosity of Anatase Thin Films Prepared by EISA: Influence of Thickness and Heat Treatment. *Microporous Mesoporous Mater.* **2009**, *117*, 292-296.

29.   Uchida, H.; Patel, M. N.; May, R. A.; Gupta, G.; Stevenson, K. J.; Johnston, K. P., Highly-Ordered Mesoporous Titania Thin Films Prepared Via Surfactant Assembly on Conductive Indium–Tin-Oxide/Glass Substrate and Its Optical Properties. *Thin Solid Films* **2010**, *518*, 3169-3176.

30.   Carreon, M. A.; Choi, S. Y.; Mamak, M.; Chopra, N.; Ozin, G. A., Pore Architecture Affects Photocatalytic Activity of Periodic Mesoporous Nanocrystalline Anatase Thin Films. *J. Mater. Chem.* **2007**, *17*, 82-89.

25

31. Wang, J.; Li, H.; Li, H.; Zou, C.; Wang, H.; Li, D., Mesoporous TiO2 Thin Films Exhibiting Enhanced Thermal Stability and Controllable Pore Size: Preparation and Photocatalyzed Destruction of Cationic Dyes. *ACS Appl. Mater. Interfaces* **2014**, *6*, 1623-1631.

32. Anderson, A.-L.; Binions, R., The Effect of Brij® Surfactants in Sol–Gel Processing for the Production of TiO2 Thin Films. *Polyhedron* **2015**, *85*, 83-92.

33. Innocenzi, P.; Malfatti, L.; Kidchob, T.; Grosso, D., Controlling the Processing of Mesoporous Titania Films by in Situ Ftir Spectroscopy: Getting Crystalline Micelles into the Mesopores. *J. Phys. Chem. C* **2010**, *114*, 10806-10811.

34. Innocenzi, P.; Malfatti, L.; Kidchob, T.; Enzo, S.; Ventura, G. D.; Schade, U.; Marcelli, A., Correlative Analysis of the Crystallization of Sol–Gel Dense and Mesoporous Anatase Titania Films. *J. Phys. Chem. C* **2010**, *114*, 22385-22391.

35. Zhou, H.; Wang, C.; Feng, Z.; Li, S.; Xu, B., Formation of Grid-Like Mesoporous Titania Film Via Structural Transformation and Its Surface Superhydrophilicity Conversion. *Surf. Coat. Technol.* **2012**, *207*, 34-41.

36. Smarsly, B.; Grosso, D.; Brezesinski, T.; Pinna, N.; Boissière, C.; Antonietti, M.; Sanchez, C., Highly Crystalline Cubic Mesoporous TiO2 with 10-nm Pore Diameter Made with a New Block Copolymer Template. *Chem. Mater.* **2004**, *16*, 2948-2952.

37. Brezesinski, T.; Wang, J.; Polleux, J.; Dunn, B.; Tolbert, S. H., Templated Nanocrystal-Based Porous Tio2 Films for Next-Generation Electrochemical Capacitors. *J. Am. Chem. Soc.* **2009**, *131*, 1802-1809.

38. Das, S.; Wu, Q.; Garlapalli, R. K.; Nagpure, S.; Strzalka, J.; Jiang, Z.; Rankin, S. E., In-Situ Gisaxs Investigation of Pore Orientation Effects on the Thermal Transformation Mechanism in Mesoporous Titania Thin Films. *J. Phys. Chem. C* **2013**, *118*, 968-976.

39. Blanc, L.; Tetelin, A.; Boissiere, C.; Tortissier, G.; Dejous, C.; Rebiere, D., Love Wave Characterization of the Shear Modulus Variations of Mesoporous Sensitive Films During Vapor Sorption. *Sensors Journal, IEEE* **2012**, *12*, 1442-1449.

40. Rahman, T.; Liu, R.; Ortel, E.; Kraehnert, R.; Antoniou, A., Mechanical Behavior of Mesoporous Titania Thin Films. *Appl. Phys. Lett.* **2014**, *104*, 241902.

41. Fuertes, M. C.; Marchena, M.; Marchi, M. C.; Wolosiuk, A.; Soler Illia, G. J. A. A., Controlled Deposition of Silver Nanoparticles in Mesoporous Single- or Multilayer Thin Films: From Tuned Pore Filling to Selective Spatial Location of Nanometric Objects. *Small* **2009**, *5*, 272-280.

42. Kirsch, B. L.; Richman, E. K.; Riley, A. E.; Tolbert, S. H., In-Situ X-Ray Diffraction Study of the Crystallization Kinetics of Mesoporous Titania Films. *J. Phys. Chem. B* **2004**, *108*, 12698-12706.

43. Forouhi, A. R.; Bloomer, I. I., Optical Dispersion Relations for Amorphous Semiconductors and Amorphous Dielectrics. *Phys. Rev. B: Condens. Matter* **1986**, *34*, 7018-7026.

44. Boissière, C.; Grosso, D.; Lepoutre, S.; Nicole, L.; Bruneau, A. B.; Sanchez, C., Porosity and Mechanical Properties of Mesoporous Thin Films Assessed by Environmental Ellipsometric Porosimetry. *Langmuir* **2005**, *21*, 12362-12371.

45. Fischer-Cripps, A. C., A Review of Analysis Methods for Sub-Micron Indentation Testing. *Vacuum* **2000**, *58*, 569-585.

46. Fischer-Cripps, A. C., *Nanoindentation*, 3rd Edition ed.; Springer, 2011.

47. Mayo, M. J.; Nix, W. D., A Micro-Indentation Study of Superplasticity in Pb, Sn, and Sn-38 Wt% Pb. *Acta Metall.* **1988**, *36*, 2183-2192.

48. Lucas, B. N.; Oliver, W. C., Indentation Power-Law Creep of High-Purity Indium. *Metall. Mater. Trans. A* **1999**, *30*, 601-610.

49. Kruk, M.; Jaroniec, M., Gas Adsorption Characterization of Ordered Organic–Inorganic Nanocomposite Materials. *Chem. Mater.* **2001**, *13*, 3169-3183.

50. Roque-Malherbe, R., *Adsorption and Diffusion in Nanoporous Materials* CRC Press, 2007.

26

51.   Carboni, D.; Marongiu, D.; Rassu, P.; Pinna, A.; Amenitsch, H.; Casula, M.; Marcelli, A.; Cibin, G.; Falcaro, P.; Malfatti, L.; Innocenzi, P., Enhanced Photocatalytic Activity in Low-Temperature Processed Titania Mesoporous Films. *J. Phys. Chem. C* **2014**, *118*, 12000-12009.

52.   Ma, W.; Lu, Z.; Zhang, M., Investigation of Structural Transformations in Nanophase Titanium Dioxide by Raman Spectroscopy. *Appl. Phys. A* **1998**, *66*, 621-627.

53.   Xie, H.; Li, N.; Liu, B.; Yang, J.; Zhao, X., Role of Sodium Ion on TiO2 Photocatalyst: Influencing Crystallographic Properties or Serving as the Recombination Center of Charge Carriers? *J. Phys. Chem. C* **2016**, *120*, 10390-10399.

54.   Ohsaka, T.; Izumi, F.; Fujiki, Y., Raman Spectrum of Anatase, TiO2. *J. Raman Spectrosc.* **1978**, *7*, 321-324.

55.   Balaji, S.; Djaoued, Y.; Robichaud, J., Phonon Confinement Studies in Nanocrystalline Anatase-Tio2 Thin Films by Micro Raman Spectroscopy. *J. Raman Spectrosc.* **2006**, *37*, 1416-1422.

56.   Doss, C. J.; Zallen, R., Raman Studies of Sol-Gel Alumina: Finite-Size Effects in Nanocrystalline Alo(Oh). *Phys. Rev. B: Condens. Matter* **1993**, *48*, 15626-15637.

57.   Yaghoubi, H.; Taghavinia, N.; Alamdari, E. K.; Volinsky, A. A., Nanomechanical Properties of Tio2 Granular Thin Films. *ACS Appl. Mater. Interfaces* **2010**, *2*, 2629-2636.

58.   Siegel, R. W., Synthesis and Properties of Nanophase Materials. *Mater. Sci. Eng., A* **1993**, *168*, 189-197.

59.   *Nanophase Materials. Synthesis, Properties, Applications*; Springer 1994.

60.   Fan, H.; Hartshorn, C.; Buchheit, T.; Tallant, D.; Assink, R.; Simpson, R.; Kissel, D. J.; Lacks, D. J.; Torquato, S.; Brinker, C. J., Modulus-Density Scaling Behaviour and Framework Architecture of Nanoporous Self-Assembled Silicas. *Nat Mater* **2007**, *6*, 418-423.

61.   Carter, C. B.; Norton, M. G., *Ceramic Materials. Science and Engineering.*, Second ed.; Springer, 2013.

62.   Karch, J.; Birringer, R.; Gleiter, H., Ceramics Ductile at Low Temperature. *Nature* **1987**, *330*, 556-558.

63.   Mayo, M. J.; Siegel, R. W.; Liao, Y. X.; Nix, W. D., Nanoindentation of Nanocrystalline Zno. *J. Mater. Res.* **1992**, *7*, 973-979.

64.   Mayo, M. J.; Siegel, R. W.; Narayanasamy, A.; Nix, W. D., Mechanical Properties of Nanophase TiO2 as Determined by Nanoindentation. *J. Mater. Res.* **1990**, *5*, 1073-1082.

65.   Maier, V.; Durst, K.; Mueller, J.; Backes, B.; Höppel, H. W.; Göken, M., Nanoindentation Strain-Rate Jump Tests for Determining the Local Strain-Rate Sensitivity in Nanocrystalline Ni and Ultrafine-Grained Al. *J. Mater. Res.* **2011**, *26*, 1421-1430.

66.   Maier, V.; Merle, B.; Göken, M.; Durst, K., An Improved Long-Term Nanoindentation Creep Testing Approach for Studying the Local Deformation Processes in Nanocrystalline Metals at Room and Elevated Temperatures. *J. Mater. Res.* **2013**, *28*, 1177-1188.

27

Table of Contents

Mesoporous TiO$_2$

Mechanical properties